Supplementary Information

Energy-generating smart windows based on the reversible metal electrodeposition

Hailin Yu[a], Liutao Chen[b], Jiayu Wang*[a], Chunxiong Bao[c], Yang Liu[d], Yuanhao Li[a], Yating Mo[a], Yingyue Hu[a], Nakul Jain[e], Xi He[a], Yinghan Wang[a], Qichao Ran[a], Cenqi Yan[a], Zhe Wang[b], Borong Lin[f], Yinhua Zhou[d], Feng Gao*[e], Pei Cheng*[a]

[a] College of Polymer Science and Engineering, State Key Laboratory of Advanced Polymer Materials, Sichuan University, Chengdu, China

[b] Department of Civil and Environmental Engineering, The Hong Kong University of Science and Technology, Hong Kong, China

[c] National Laboratory of Solid State Microstructures, School of Physics, Nanjing University, Nanjing, China

[d] Wuhan National Laboratory for Optoelectronics, Huazhong University of Science and Technology, Wuhan, China

[e] Department of Physics, Chemistry and Biology (IFM), Linköping University, Linköping, Sweden

[f] Department of Building Science, School of Architecture, Tsinghua University, Beijing, China

*Email: wangjiayu@scu.edu.cn (J.W.); feng.gao@liu.se (F.G.); chengpei@scu.edu.cn (P.C.)

Experimental Section

1. Materials

PM6 and BTP-eC9 were purchased from the Solarmer (Beijing). 1,8-diiodooctane and D-sorbitol were acquired from Sigma-Aldrich. PH1000 was obtained from Heraeus. PEDOT:F was synthesized according to literature.[S1] Chlorobenzene, $Zn(CH_3COO)_2 \cdot 2H_2O$, 2-methoxyethanol and ethanolamine were purchased from J&K Scientific. $CuCl_2$, $BiCl_3$ and LiBr were acquired from Adamas. Polyvinyl alcohol and dilute hydrochloric acid were purchased from Aladdin. All chemicals were used without further purification.

2. Preparation of ECDs

ECDs were fabricated by sandwiching a butyl rubber sealing ring between an ITO glass and a regular glass with Cu foil sticked at the edges. The thickness of the sealing ring is 3 mm and the width is 3 mm. 0.202 g $CuCl_2$, 0.158 g $BiCl_3$ and 8.69 g LiBr were dissolved in 90 mL deionized water at room temperature, followed by adding 84 μL hydrochloric acid (36%) dropwise to obtain solution A. 0.15 g polyvinyl alcohol (M_W = 44000) was dissolved in 10 mL deionized water at 90 °C to obtain solution B. Afterward, solution A and solution B were mixed and stirred at room temperature to obtain the electrolyte. The electrolyte was injected into the ECD by syringe. The total thickness of ECD was 5.2 mm.

3. Fabrication of large-area laminated STOPVs

The glass/ITO substrates were sequentially cleaned in an ultrasonic bath of detergent, deionized water, acetone and isopropyl alcohol for 15 minutes each. ZnO was spin-

coated onto the substrate from a precursor (100mg $Zn(CH_3COO)_2 \cdot 2H_2O$ and 0.02 mL ethanolamine dissolved in 1 mL 2-methoxyethanol) and baked on a hotplate at 200 ℃ for 60 minutes. The active layer was spin-coated on ZnO from a chlorobenzene solution of PM6:BTP-eC9 (10:12, 7.5:12, 5:12 or 2.5:12 mg mL^{-1}) with 0.7% (v/v) 1,8-diiodooctane as solvent additive at 2700 rpm, and annealed at 100 °C for 5 minutes. PEDOT:F was spin-coated onto the active layer at 2000 rpm and annealed at 100 °C for 2 minutes. In parallel, transparent conductive adhesive,[S2, S3] which was prepared by mixing PEDOT:PSS PH1000 (1 mL) and D-sorbitol (400 mg), was spin-coated on ITO substrate and annealed at 110 ℃ for 10 minutes. Finally, the two half-stacks were laminated by double-clip pressing and subsequently dried at 105 ℃ for 10 min.

4. Self-powered energy-saving smart windows

The double-sided ITO glass substrates were sequentially cleaned in an ultrasonic bath of detergent, deionized water, acetone and isopropyl alcohol for 15 minutes each. STOPV sub-device was first fabricated through the above procedures. The other side of ITO was swiped with deionized water and isopropyl alcohol, and the electrochromic sub-device was fabricated through the above procedures. The two sub-devices were connected via a microcontroller and the circuit diagram is presented in **Fig. S13.**

5. Characterizations

The *J–V* characteristics were measured using a Keysight B2901A source meter under the illumination of an Enlitech solar simulator (SS-X50, AAA grade) coupled with AM 1.5G solar spectrum filters. The optical power at the device was calibrated as 100 mW cm^{-2} using a polycrystalline silicon reference cell (SRC2020). The devices were

measured by masking the active area with a metal aperture. The EQE spectra were measured using a Solar Cell Spectral Response Measurement System QE-R (Enlitech Co., Ltd.). Ultraviolet photoelectron spectroscopy (UPS) was performed on a PHI 5000 VersaProbe III photoelectron spectrometer with He I source (21.22 eV) under an applied negative bias of 9.0 V. Absorption, transmittance and reflectance spectra were recorded on a Shimadzu UV-2600i spectrophotometer at room temperature. Testing of ECDs was conducted on a CHI660E electrochemistry workstation. The cyclic voltammetry test was scanned at a rate of 20 mV s^{-1}. A voltage of −0.7 V (versus Cu foil) is applied to the ECDs for Cu-Bi alloy deposition, and a voltage of 0.7 V (versus Cu foil) is applied to the ECDs for bleaching. The pulse duration and response time for coloring/blenching of cyclic stability test is 120 s, 80 s for coloring as well as 60 s for blenching. The voltage switching conditions is as follows: when solar irradiance exceeds or falls below 40 mW cm^{-2}, the polarity of the voltage applied to the electrochromic device automatically switches. Self-powered energy-saving smart windows between its clear and tinted states were tested in ambient air under a solar simulator (SCX-100, Zhongkeshicheng Technology). An aluminum foil wrapped chamber (13 cm × 11 cm × 11 cm) with an aperture (2.5 cm × 2.5 cm) on the top was used for temperature testing. A solar simulator (CEL-S500, 100 mW cm^{-2}) is used as light source, and infrared images and surface temperatures of the samples were recorded using a thermal infrared camera (FLIR-T600).

6. Building energy saving calculation

To evaluate the energy performance of self-powered energy-saving smart windows in diverse geographical and climatic conditions, we conducted office building energy simulations in eight locations: Bangkok (Thailand), Riyadh (Saudi Arabia), Miami (USA), New Delhi (India), Hong Kong (China), Phoenix (USA), San Diego (USA), and New York (USA). These locations represent ASHRAE climate zones 0A, 0B, 1A, 1B, 2A, 2B, 3C, and 4A, respectively. We utilized a standard office floor from the large office prototype building developed by the Pacific Northwest National Laboratory (PNNL) of the US Department of Energy (DOE) (https://www.energycodes.gov/prototype-building-models) as the basis for our simulations. The building consists of 12 stories and a basement, with the selected office floor situated at the mid-level. This floor comprises one core zone, one data center, and four perimeter zones, with gross dimensions of 73.11 m × 48.74 m and a total floor area of 3563.4 m^2. The prototype specifies a window-to-wall ratio (WWR) of 57.8%, evenly distributed among all four sides of the building, facing the cardinal directions. The floor area of the north and south perimeters is 313.4 m^2, featuring 73.11 m × 1.59 m windows on the north and south walls, respectively. The east and west perimeters have a floor area of 202.0 m^2, with 48.74 m × 1.59 m windows on the east and west walls, respectively. Thermostat setpoints are set at 24 °C for cooling and 21 °C for heating. Electric lighting in each perimeter follows a continuous lighting control, dimming continuously as daylight illuminance increases. The illuminance setpoint is 377 lux at a height of 0.76 m and distances of 1.68 m and 3.35 m from the window. Consequently, the choice of window type influences daylight illuminance levels and the electric

lighting consumption. The photovoltaic power output is simulated using EnergyPlus' simple model, which primarily correlates with incident radiation and module radiation-varying efficiency.

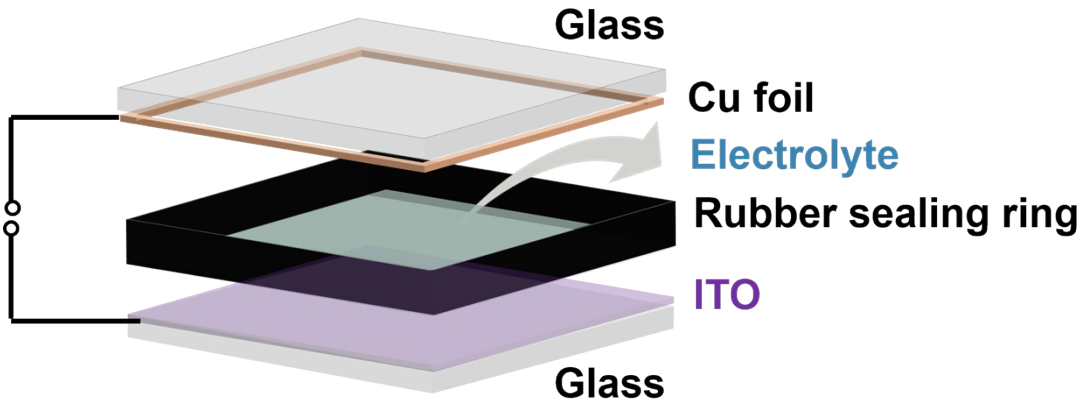

Fig. S1 Schematic of ECDs based on reversible metal electrodeposition.

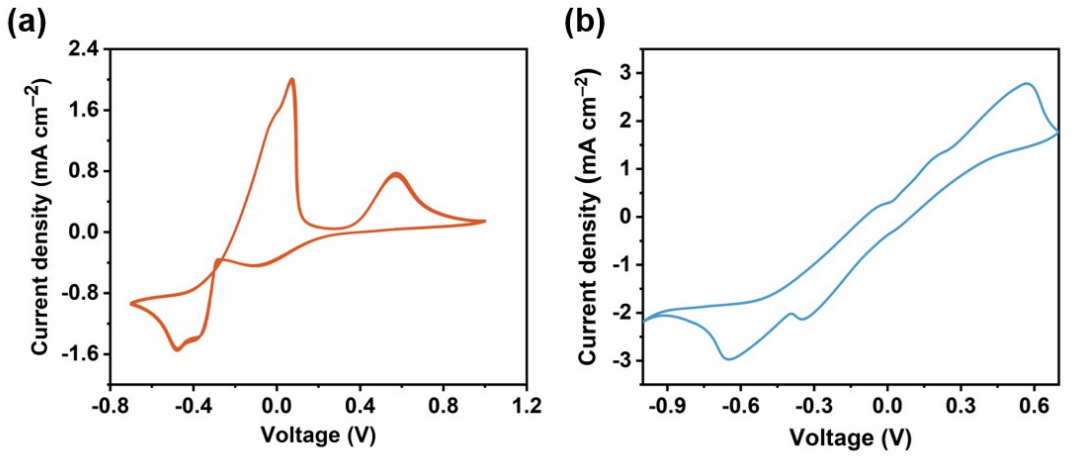

Fig. S2 The Cyclic voltammetry curves of ECDs. (a) Cyclic voltammetry curve of the ECD electrolyte. A glassy carbon electrode is used as working electrode, a platinum electrode is used as counter electrode, and an Ag/AgCl electrode is used as reference electrode. (b) Cyclic voltammetry curve of the ECD. The ITO electrode is used as working electrode, and the Cu foil is used as both counter and reference electrodes.

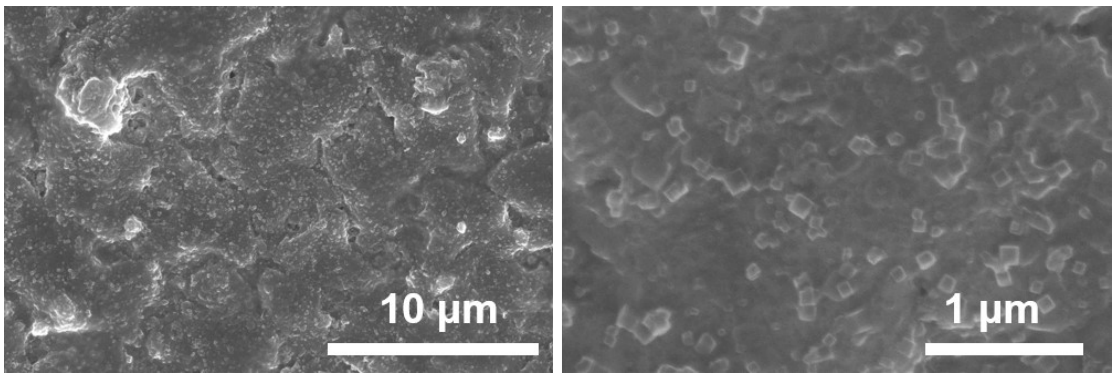

Fig. S3 SEM morphology of metal electrodeposited after 1 min with 0.2 wt% PVA dissolved in the plating solution.

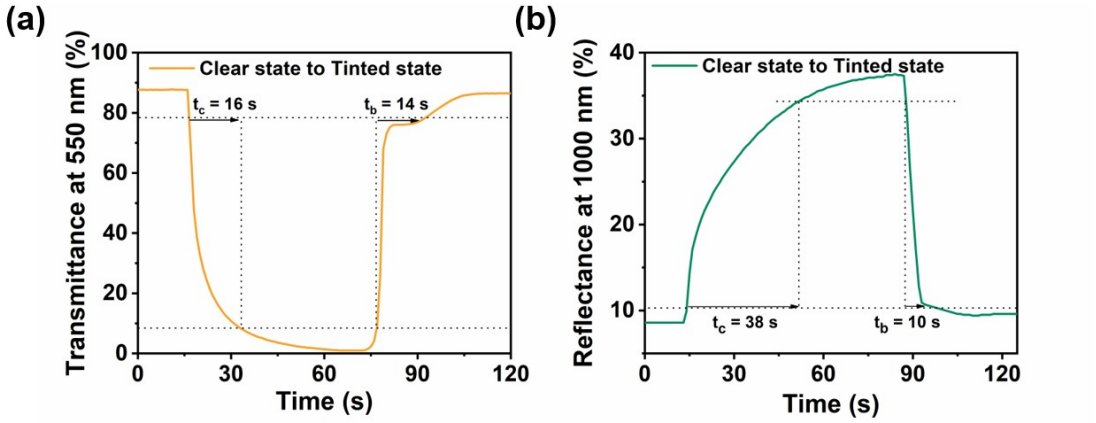

Fig. S4 (a) In-situ optical response of the ECDs with the transmittance change from clear state to tinted state. (b) Reflectance change from clear state to tinted state.

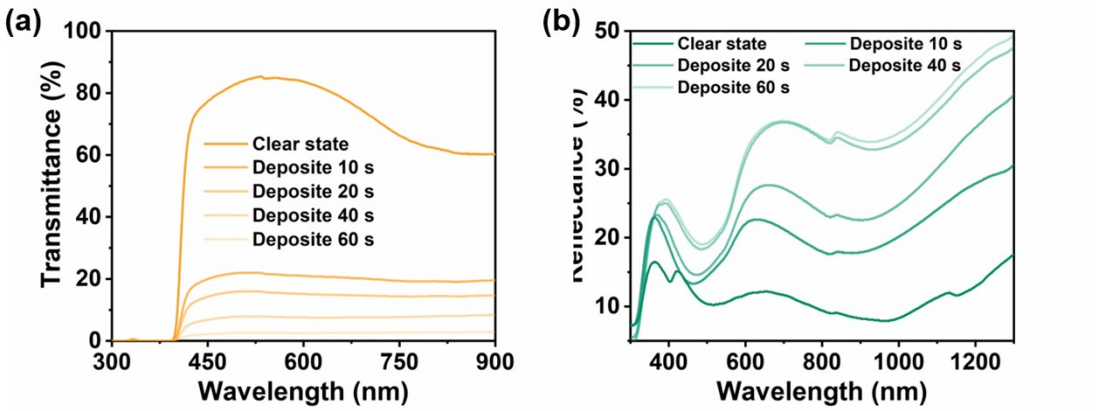

Fig. S5 (a) Transmittance spectra of ECDs for five distinct optical states and the switching times required to achieve each state. (b) Reflectance spectra measured through the ITO-on-glass electrode of ECDs for five distinct optical states.

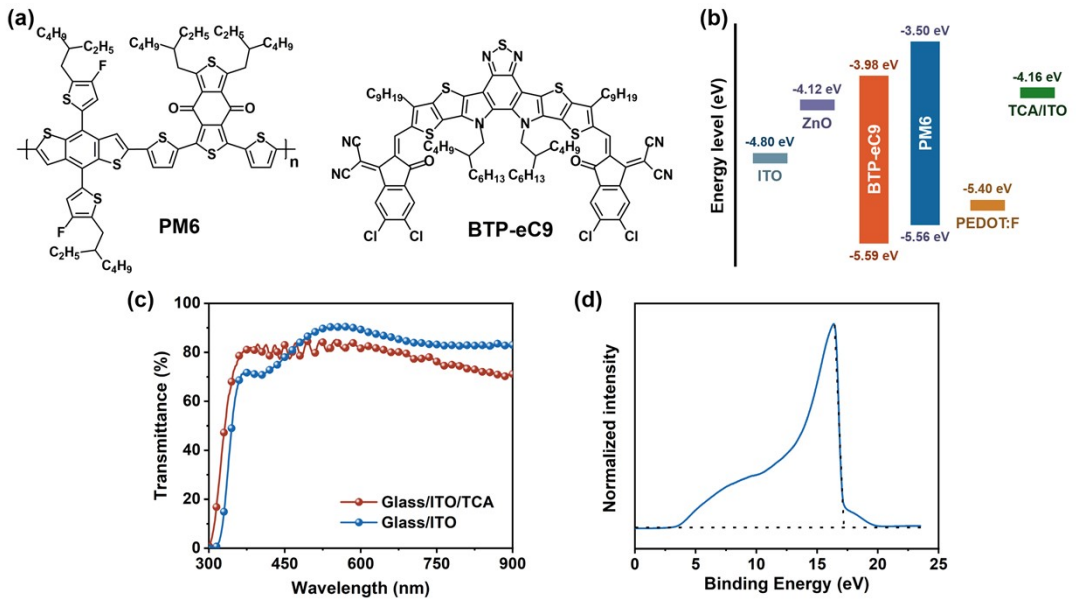

Fig. S6 (a) The chemical structures of PM6 and BTP-eC9. (b) The energy level alignment of different materials. (c) Transmittance spectra of glass/ITO and glass/ITO/transparent conductive adhesive (TCA). (d) UPS spectrum of TCA/ITO.

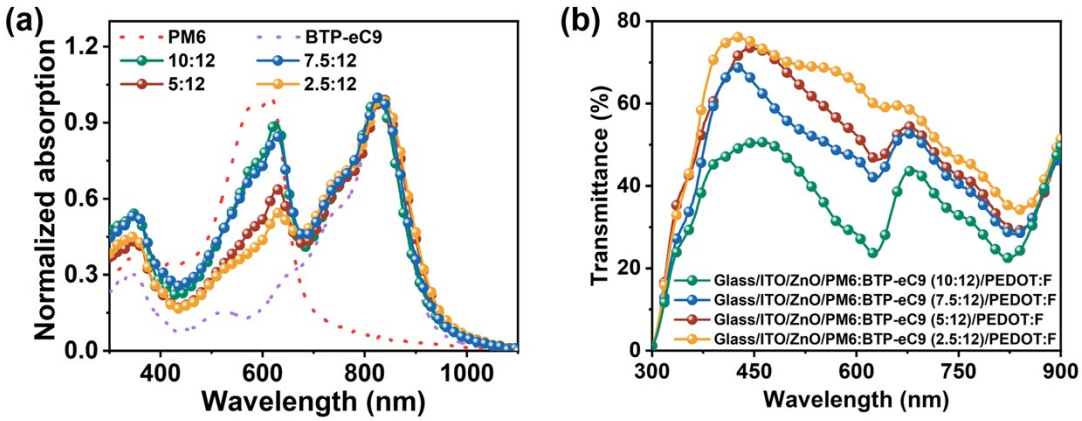

Fig. S7 (a) The normalized absorption spectra of active layer with different donor: acceptor ratios. (b) The transmittance spectra of glass/ITO/ZnO/PM6:BTP-eC9/PEDOT:F with different donor: acceptor ratios.

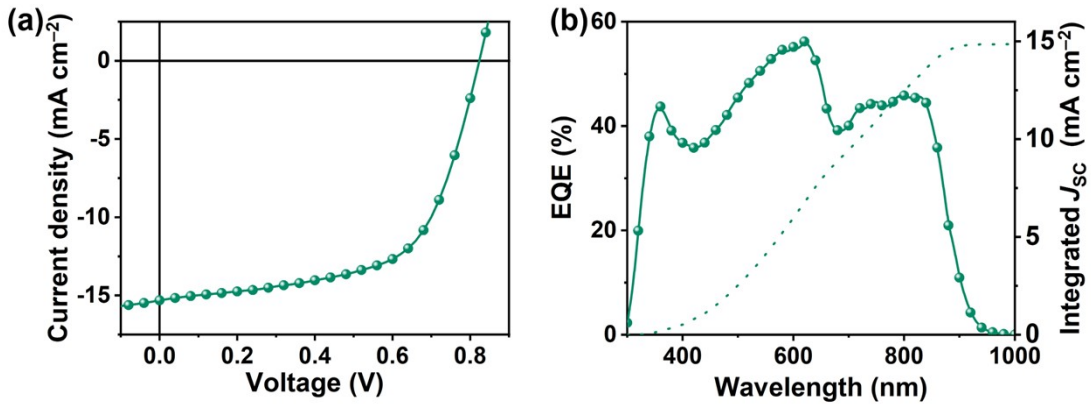

Fig. S8 (a) The *J-V* curves of the champion laminated STOPVs under simulated AM 1.5G illumination (100 mW cm^{-2}). (b) The EQE spectra of corresponding laminated STOPVs.

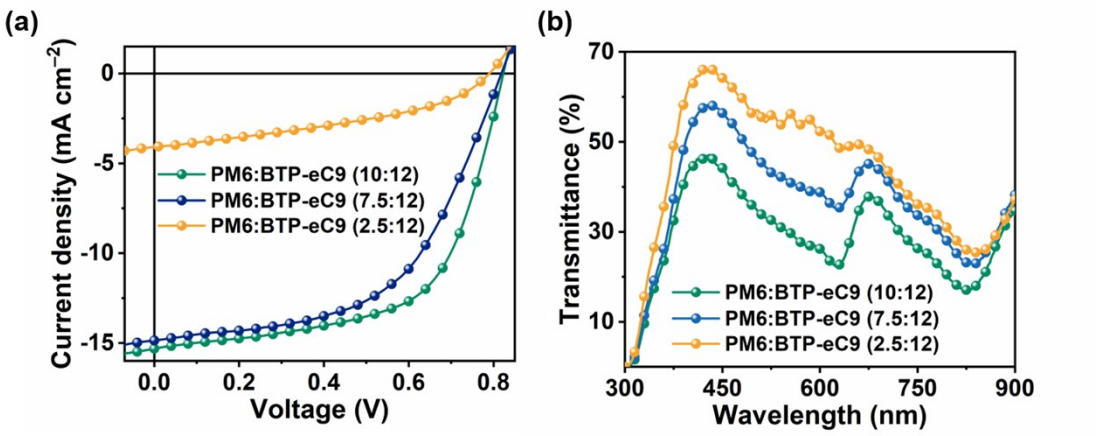

Fig. S9 (a) The *J-V* curves of STOPVs with different D:A ratio. (b) The transmittance spectra of STOPVs with different D:A ratio.

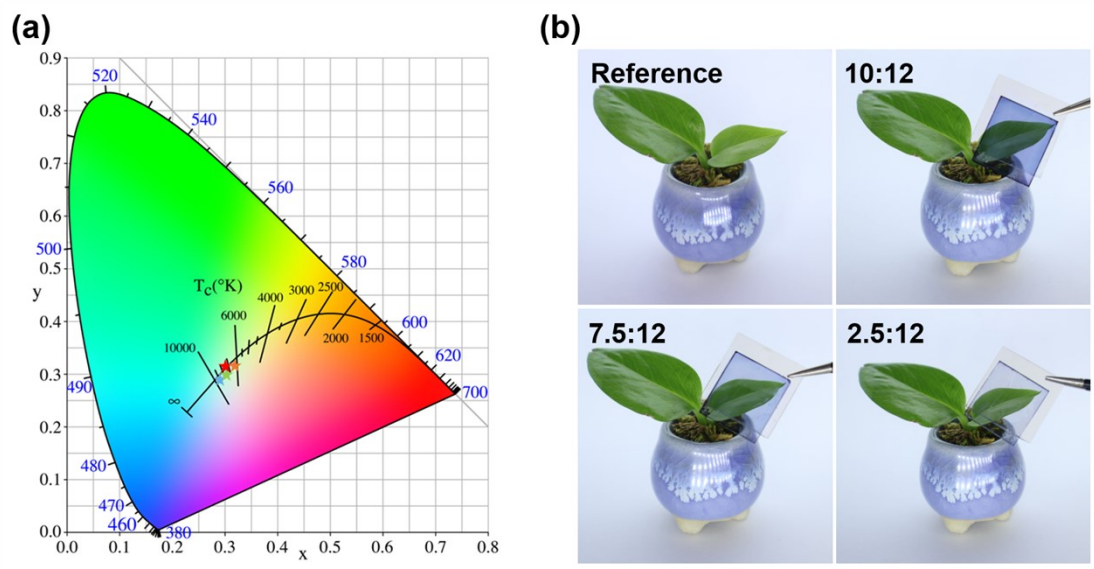

Fig. S10 The optical performance of STOPVs with different donor content. (a) The color coordinates of STOPVs with different donor content. (b) The photograph of STOPVs at different donor content.

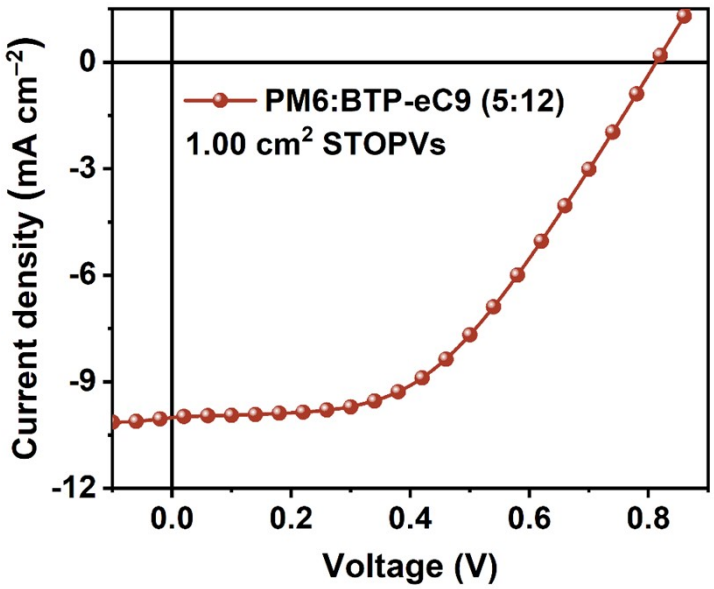

Fig. S11 The *J-V* curve of STOPVs with an area of 1.00 cm^2.

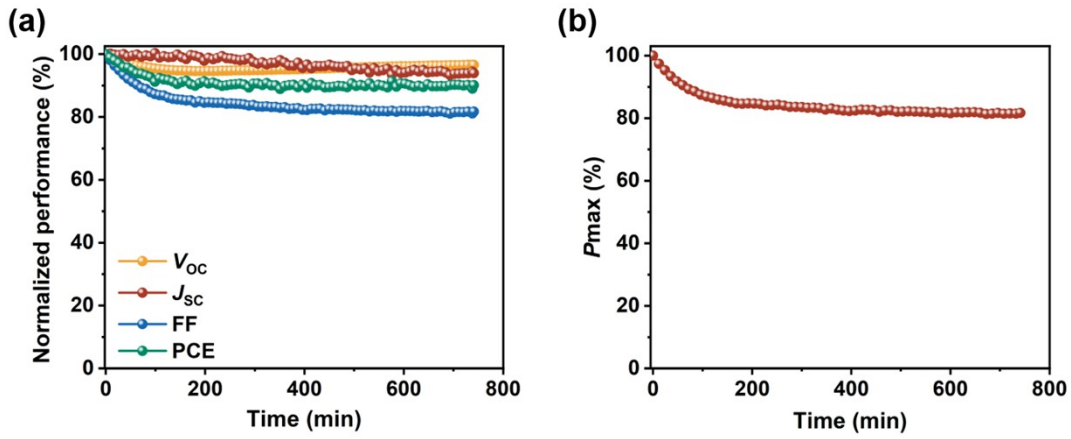

Fig. S12 The light stability performance of the unencapsulated STOPVs devices under maximum power point (MPP) tracking under AM 1.5G (100 mW cm^{-2} illumination. (a) The curves of V_{OC}, J_{SC}, FF and PCE versus time. (b) The curve of P_{max} versus time.

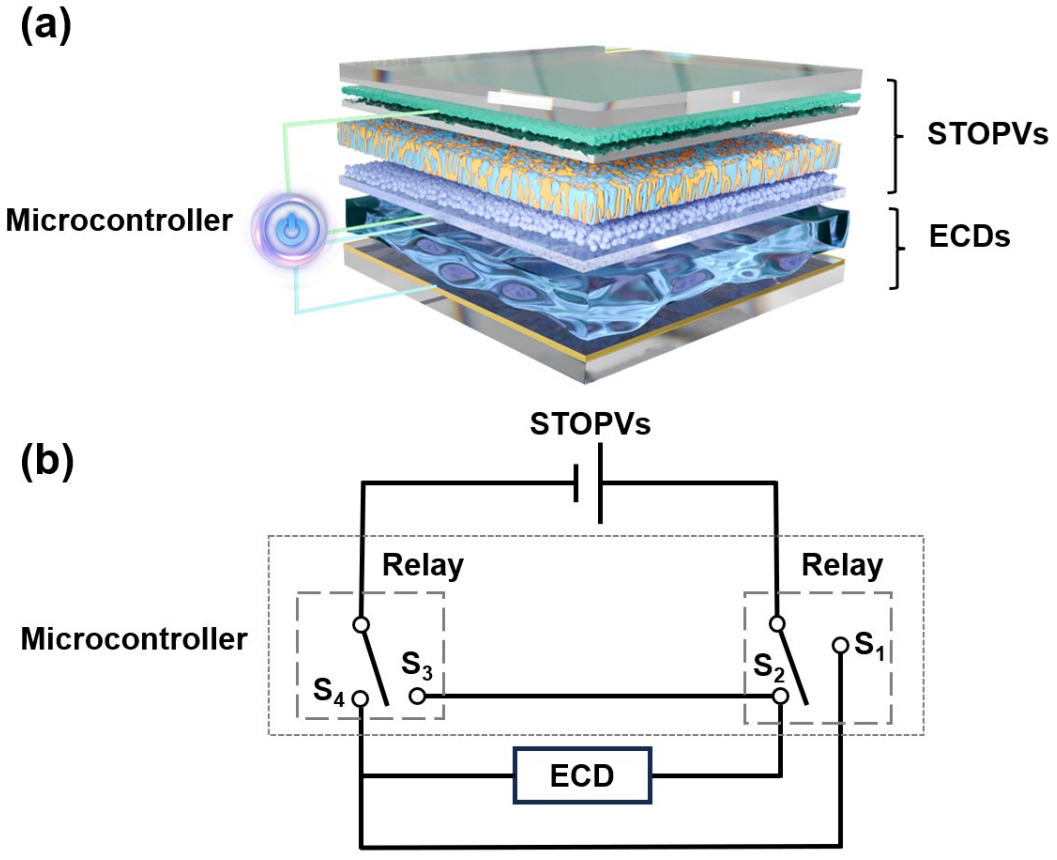

Fig. S13 (a) The main units of smart windows system consisting of STOPVs, ECDs and microcontroller. (b) The working circuitry of the smart windows system.

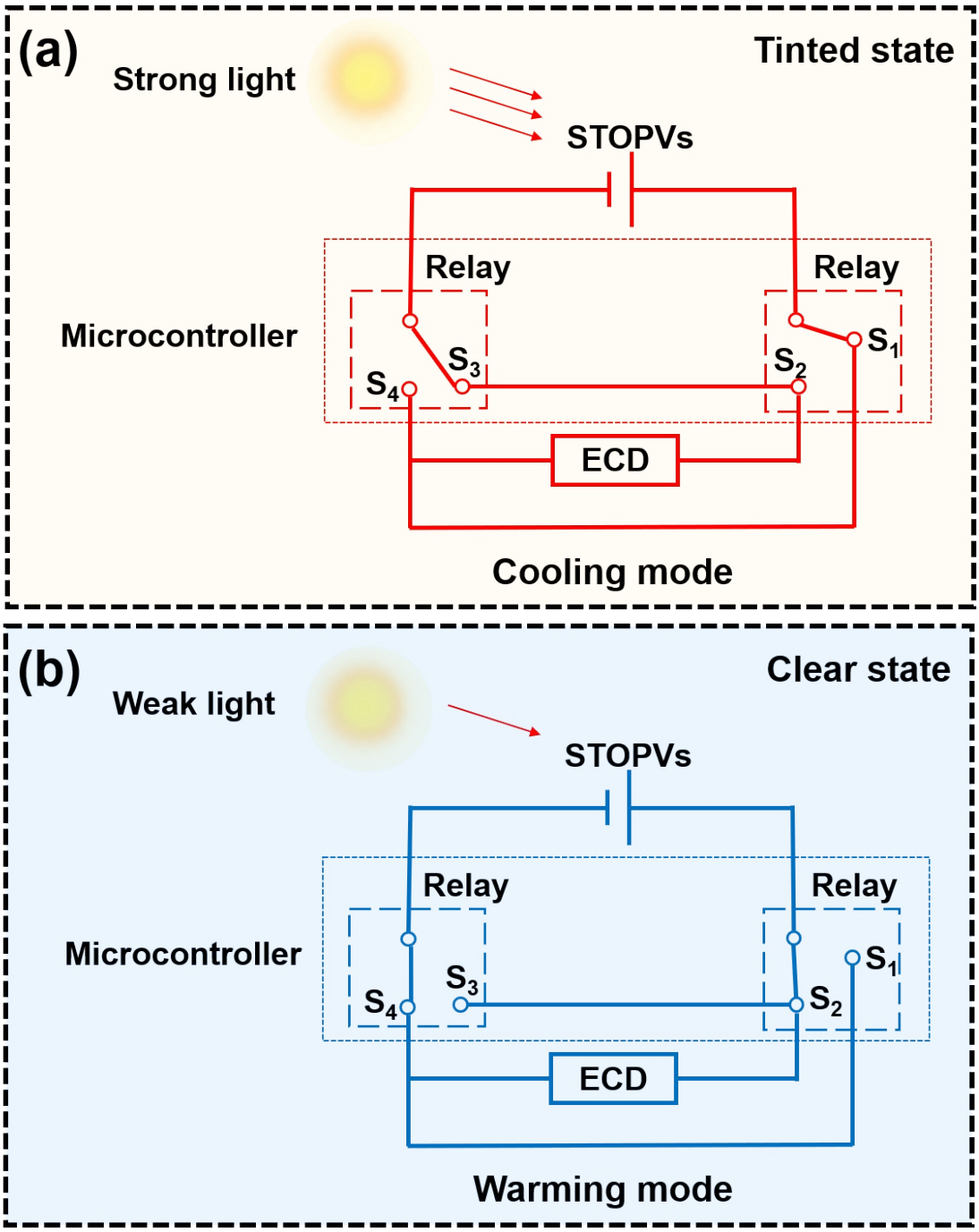

Fig. S14 Working mechanism of the smart windows system in (a) cooling and (b) warming modes. Since the output voltage of STOPVs varies with light intensity, the microcontroller detects the voltage of STOPVs and controls the voltage direction applied to ECD through relays. For example, the STOPVs show an output voltage of 0.6 V under 40 mW cm^{-2} illumination. When the light intensity exceeds 40 mW cm^{-2}, the STOPVs show an output voltage above 0.6 V and the microcontroller activate relay S_1 and S_3, connecting the ITO electrode of ECD to the cathode of STOPVs. Then, the

Cu-Bi alloy is deposited on the ITO electrode and the smart window is changed to tinted state and works in cooling mode. Conversely, when the light intensity drops below 40 mW cm^{-2}, the STOPVs outputs a voltage below 0.6 V and the microcontroller engages relay S_2 and S_4. This reverses the voltage direction applied to ECD and the Cu-Bi alloy gradually dissolved, transiting the smart window back to clear state and thereby activating warming mode.

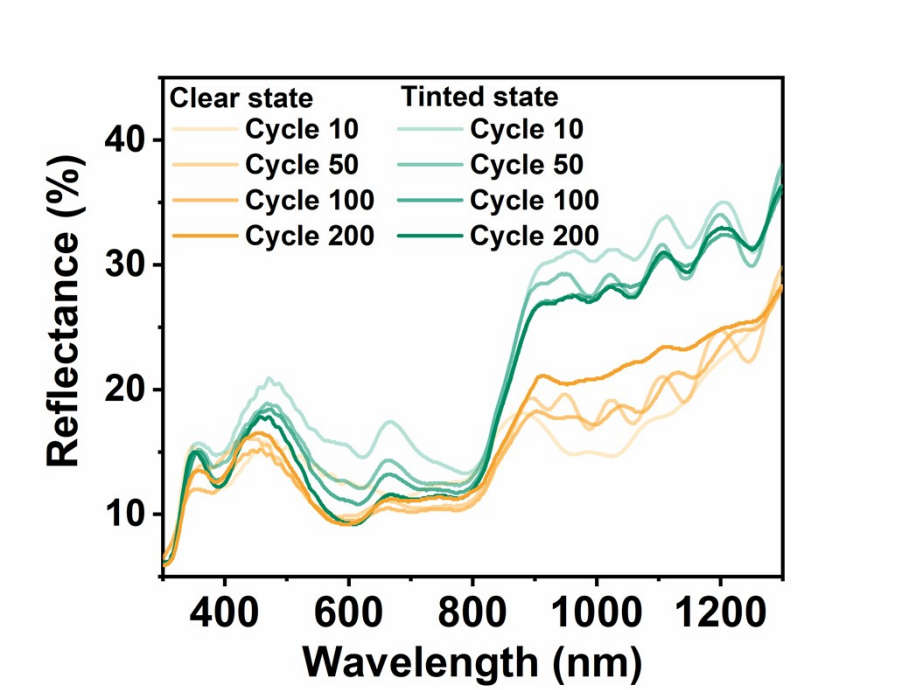

Fig. S15 Reflectance spectra of the smart windows at 10, 50, 100 and 200 cycles.

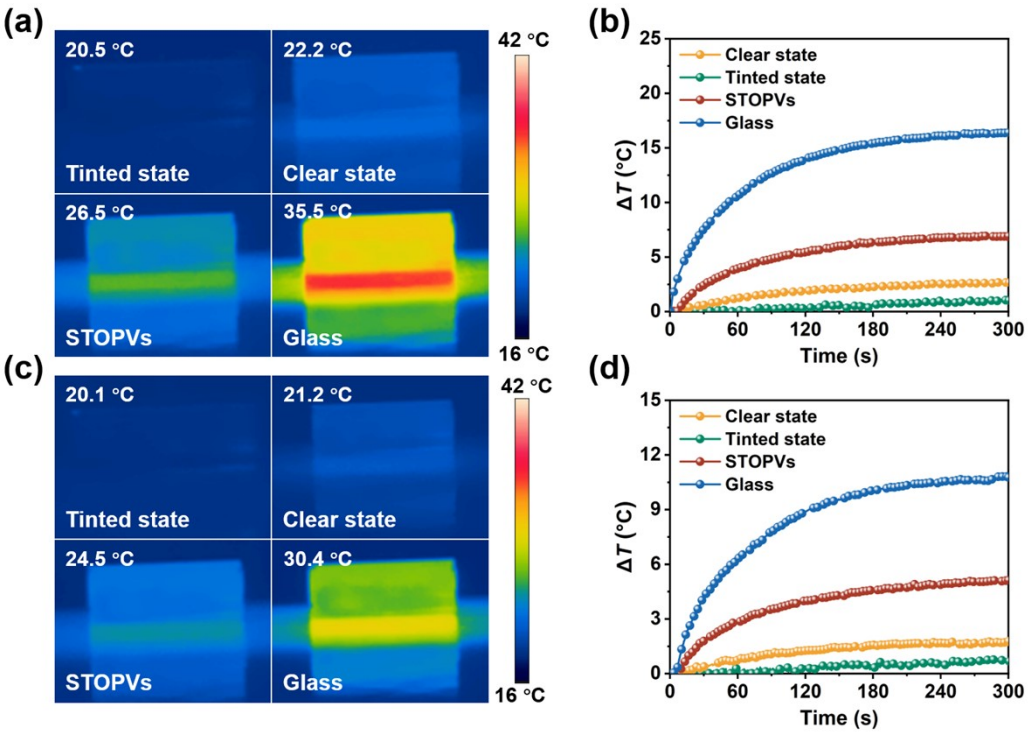

Fig. S16 The heat insulation and temperature regulation functions of different windows under different light intensity illumination. (a) infrared images and (b) temperature change of the black swallow tail clip in the chamber installed with different windows under 80 mW cm^{-2} illumination. (c) infrared images and (d) temperature change of the black swallow tail clip in the chamber installed with different windows under 40 mW cm^{-2} illumination.

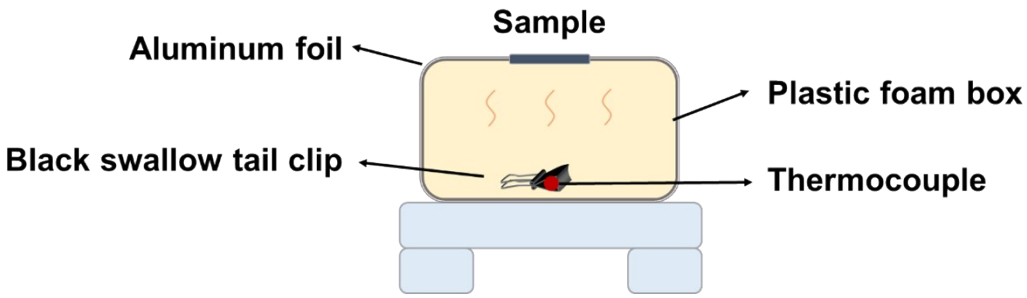

Fig. S17 Schematic of the setup built for actual cooling performance measurements.

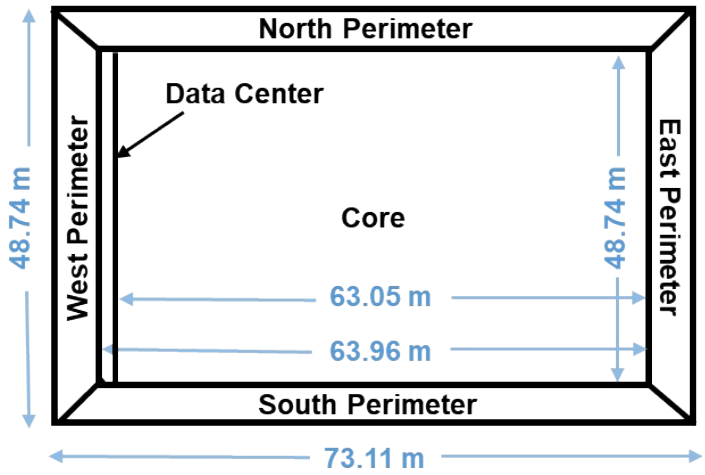

Fig. S18 Floor plan of the standard office floor.

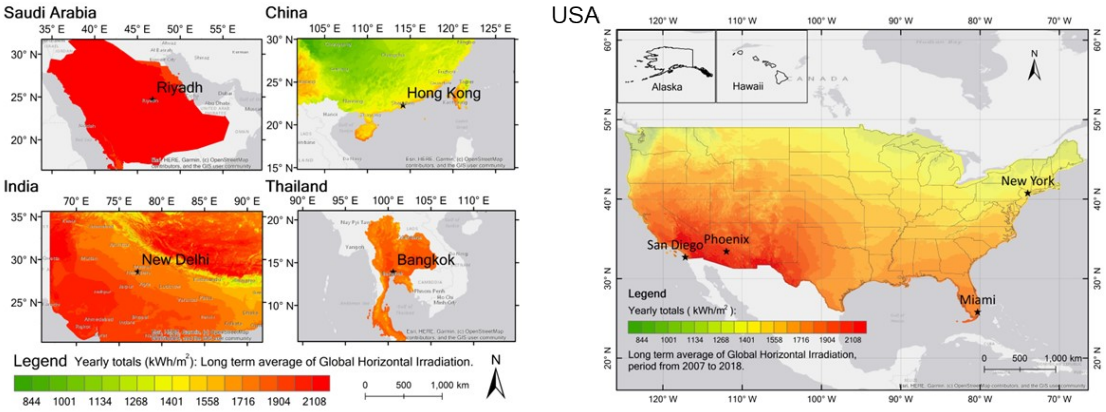

Fig. S19 Average annual global horizontal irradiation at the eight study sites from 2007 to 2018 (Solar resource data from Solargis, https://globalsolaratlas.info).

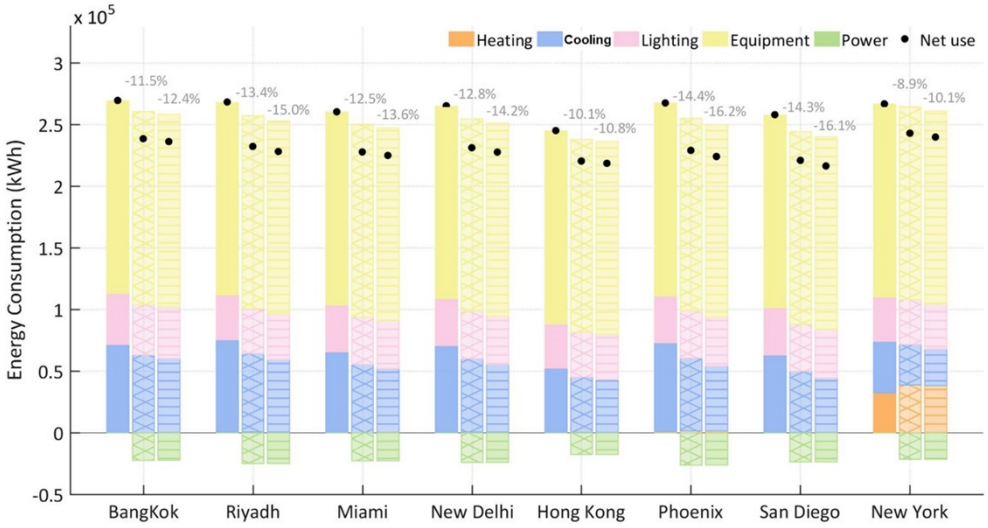

Fig. S20 Comparison of annual energy consumption of a standard office floor in eight study cities: clear glass (solid bar), STOPVs glass (bar with cross shading), and self-

powered energy-saving smart windows (bar with horizontal shading). The black dot indicates the net energy use for STOPVs and self-powered energy-saving smart windows, where generated power offsets total energy consumption. The grey texts represent the net energy saving ratio compared to the clear glass case.

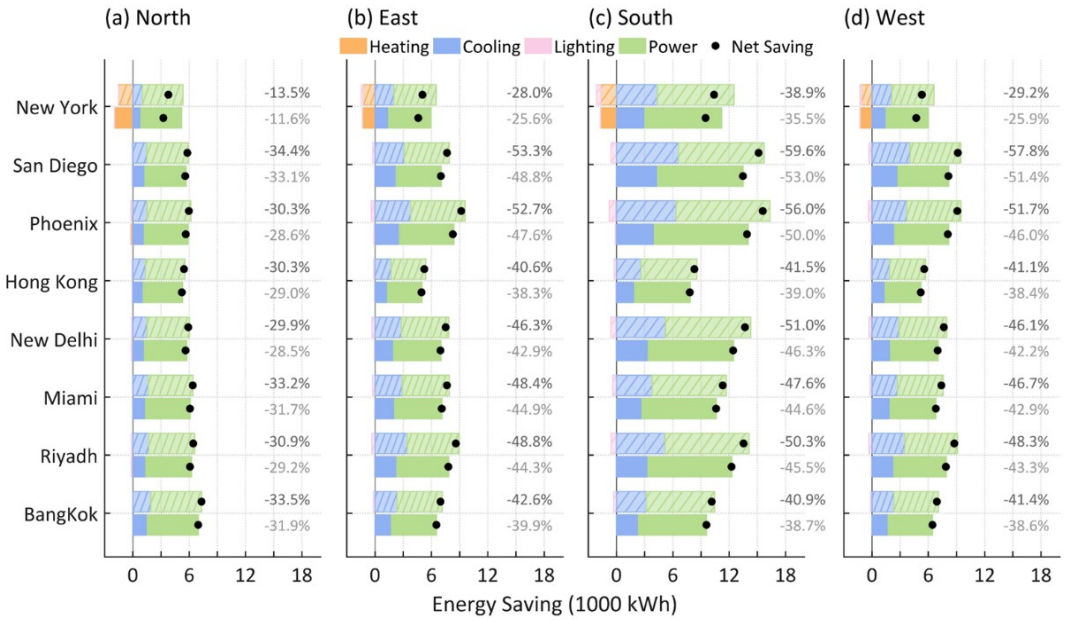

Fig. S21 Comparison of annual energy saving of (a) north, (b) east, (c) south, (d) west perimeter zones of a standard office floor equipped with STOPVs glass (solid bar) and self-powered energy-saving smart windows (shaded bar) across the eight study sites. The black dot represents the net energy savings for the STOPVs and self-powered energy-saving smart windows cases, calculated as the generated power plus the saved cooling energy minus the additional heating and lighting energy. The grey text indicates the net energy saving ratio relative to the total energy consumption of the control case (clear glass).

Table S1 The photovoltaic parameters of the laminated OPVs with different D:A ratios in this work.

D:A ratio	V_{OC} (V)	J_{SC} (mA cm^{-2})	FF (%)	PCE (%)
10:12	0.816	15.3	61.7	7.73
7.5:12	0.818	14.9	54.0	6.55
5:12	0.807	11.9	54.8	5.29
2.5:12	0.790	4.1	40.2	1.30

Table S2 The summarized photovoltaic characteristics of the laminated OPVs.

Ref.	PCE (%)	AVT (%)	Area (cm^2)
S4	3.2	25	0.4
S5	4.0	N/A	N/A
S6	3.79	N/A	N/A
S7	4.0	N/A	N/A
S8	3.7	61	0.014
S9	5.88	31	0.15
S10	3.22	53	0.056
S11	3.0	51	0.25
This work	7.73	34.4[a]	0.04
This work	6.55	45.4[a]	0.04
This work	5.29	50.7[a]	0.04
This work	1.30	55.5[a]	0.04
This work	3.86	50.7[a]	1.0

[a] AVT is the fraction of visible light, weighted by the arithmetic mean of visible light at 400-700 nm.

Table S3 The detailed weather data of the eight study sites.

City	Thermal Zone	Climate characteristics	Weather location	Yearly total irradiation (kWh/m^2)
Bangkok, Thailand	0A	Extremely Hot Humid	13.92° N, 100.60° E	1804
Riyadh, Saudi Arabia	0B	Extremely Hot Dry	24.70° N, 46.80° E	2239
Miami, USA	1A	Very Hot Humid	25.82° N, 80.30° W	1853
New Delhi, India	1B	Very Hot Dry	28.58° N, 77.20° E	1720
Hong Kong, China	2A	Hot Humid	22.32° N, 114.17° E	1458
Phoenix, USA	2B	Hot Dry	33.45° N, 111.98° W	2122
San Diego, USA	3C	Warm Marine	32.73° N, 117.17° W	1914
New York, USA	4A	Mixed Humid	40.78° N, 73.97° W	1488

References

S1. Y. Jiang, X. Dong, L. Sun, T. Liu, F. Qin, C. Xie, P. Jiang, L. Hu, X. Lu, X. Zhou, W. Meng, N. Li, C. J. Brabec, Y. Zhou, *Nat. Energy,* 2022, **7**, 352.

S2. J. Huang, G. Li, Y. Yang, *Adv. Mater.,* 2008, **20**, 415.

S3. G. D. Spyropoulos, C. O. Ramirez Quiroz, M. Salvador, Y. Hou, N. Gasparini, P. Schweizer, J. Adams, P. Kubis, N. Li, E. Spiecker, T. Ameri, H.-J. Egelhaaf, C. J. Brabec, *Energy Environ. Sci.,* 2016, **9**, 2302.

S4. J. Huang, G. Li, Y. Yang, *Adv. Mater.,* 2008, **20**, 415.

S5. Y. Yuan, Y. Bi, J. Huang, *Appl. Phys. Lett*., 2011, **98**, 063306.

S6. Y. Lu, C. Alexander, Z. Xiao, Y. Yuan, R. Zhang, J. Huang, *Nanotechnology,* 2012 **23**, 344007.

S7. L. Yin, Z. Zhao, F. Jiang, Z. Li, S. Xiong, Y. Zhou, *Org. Electron.,* 2014, **15**, 2593.

S8. Y. Song, S. Chang, S. Gradecak, J. Kong, *Adv. Energy Mater.,* 2016, **6**, 1600847.

S9. G. D. Spyropoulos, C. O. Ramirez Quiroz, M. Salvador, Y. Hou, N. Gasparini, P. Schweizer, J. Adams, P. Kubis, N. Li, E. Spiecker, T. Ameri, H.-J. Egelhaaf, C. J. Brabec, *Energy Environ. Sci.,* 2016, **9**, 2302.

S10. Y. Wang, B. Jia, F. Qin, Y. Wu, W. Meng, S. Dai, Y. Zhou, X. Zhan, *Polymer,* 2016, **107**, 108.

S11. M. Makha, P. Testa, S. B. Anantharaman, J. Heier, S. Jenatsch, N. Leclaire, J. N. Tisserant, A. C. Veron, L. Wang, F. Nuesch, R. Hany, *Sci. Technol. Adv. Mater.,* 2017, **18**, 68.